Development and implementation of a high-resolution dynamical wall and roof model for ENVI-met

Part 1:
General model design and
non-vegetated walls and roofs

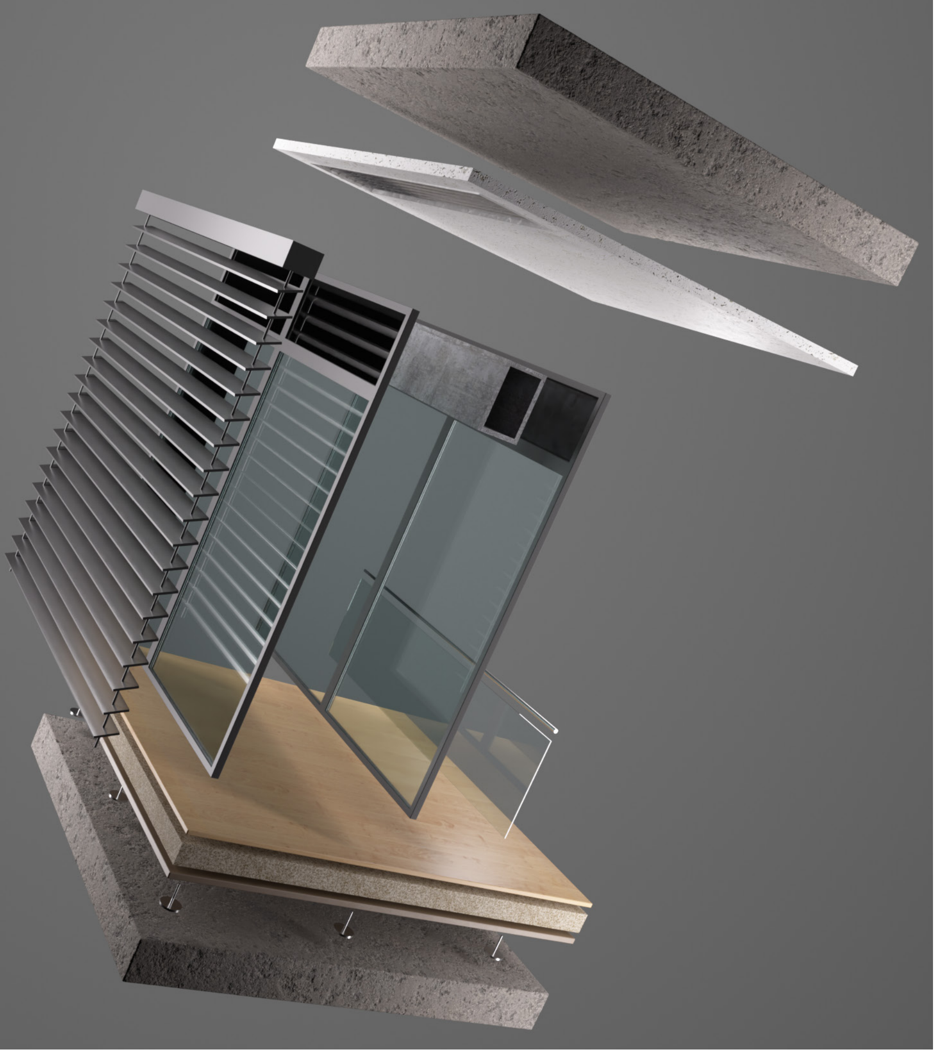

Michael Bruse, Helge Simon and Tim Sinsel
2023

Development and implementation of a high-resolution dynamical wall and roof model for ENVI-met

Part 1: General model design and non-vegetated walls and roofs

Edition 2023.1

Michael Bruse, Helge Simon and Tim Sinsel

Glossary

Symbol	Description	Unit
Radiation		
$Q^{\mathrm{W}}_{\mathrm{SW,net}}$	Net absorbed shortwave radiation	$\left[\mathrm{W\,m^{-2}}\right]$
$Q^{\mathrm{W}}_{\mathrm{LW,net}}$	Longwave radiation budget	$\left[\mathrm{W\,m^{-2}}\right]$
$Q_{\mathrm{SW,dir}}$	Incoming direct shortwave radiation	$\left[\mathrm{W\,m^{-2}}\right]$
$Q_{\mathrm{SW,dif}}$	Incoming diffuse shortwave radiation	$\left[\mathrm{W\,m^{-2}}\right]$
$Q_{\mathrm{SW,refl}}$	Incoming reflected shortwave radiation	$\left[\mathrm{W\,m^{-2}}\right]$
Q_{LW}	Incoming longwave radiation	$\left[\mathrm{W\,m^{-2}}\right]$
$Q^{\mathrm{ret}}_{\mathrm{SW,dif}}$	Diffuse shortwave radiation returned from wall	$\left[\mathrm{W\,m^{-2}}\right]$
$Q^{\mathrm{W}}_{\mathrm{LW,out}}$	Longwave radiation emitted from the building wall	$\left[\mathrm{W\,m^{-2}}\right]$
Microclimate		
$\mathbf{u}$	Tangential Wind speed in front of façade	$\left[\mathrm{m\,s^{-1}}\right]$
T_{a}	Air temperature in front of wall	$[\mathrm{K}]$
T_{indoor}	Building indoor temperature	$[\mathrm{K}]$
T_{i}	Wall temperature of node i (e.g.$i = 0$ outside, $i = 6$ inside)	$[\mathrm{K}]$
Other Symbols		
H^{W}	Sensible heat flux	$\left[\mathrm{W\,m^{-2}}\right]$
LE^{W}	Latent heat flux	$\left[\mathrm{W\,m^{-2}}\right]$
G^{W}	Conduction heat flux	$\left[\mathrm{W\,m^{-2}}\right]$
τ_{M}	Absorption coefficient for shortwave radiation	$[-]$
α_{W}	Shortwave albedo	$[-]$
ε_{W}	Longwave emissivity	$[-]$
λ_{W}	Heat conductivity	$\left[\mathrm{W\,K^{-1}\,m^{-1}}\right]$
β	Angle between façade or roof normal and sun	$[^\circ]$
h_c	Heat transfer coefficient at the wall outside	$\left[\mathrm{W\,m^{-2}\,K^{-1}}\right]$
h_i	Heat transfer coefficient at the wall inner side	$\left[\mathrm{W\,m^{-2}\,K^{-1}}\right]$
c_{D}	Drag coefficient	$[-]$
z_0	Roughness length	$[\mathrm{m}]$
S_θ	Heat exchange with main atmosphere model	$\left[\mathrm{K\,s^{-1}}\right]$
Δt	Time step length	$[\mathrm{s}]$
$\Delta x, \Delta y, \Delta z$	Grid cell resolutions in x, y, and z direction	$[\mathrm{m}]$
Δ_{W}	Half the thickness of neighbouring model grid cell	$[\mathrm{m}]$
Δ_{i}	Distance between calculation nodes of the wall	$[\mathrm{m}]$
Constants		
c_p	Specific heat capacity of air = $1005\,\mathrm{J\,K^{-1}\,kg^{-1}}$	$\left[\mathrm{J\,K^{-1}\,kg^{-1}}\right]$
ρ_a	Density of air at $20\,^\circ\mathrm{C} = 1.29\,\mathrm{kg\,m^{-3}}$	$\left[\mathrm{kg\,m^{-3}}\right]$
κ	Von Karman constant = 0.4	$[-]$
σ_B	Stefan-Boltzmann constant = $5.67 \times 10^{-8}\,\mathrm{W\,m^{-2}\,K^{-4}}$	$\left[\mathrm{W\,m^{-2}\,K^{-4}}\right]$

1 Introduction

1.1 Background

Wall and roof temperatures have a crucial impact on the urban microclimate both during the day and at night. This is primarily due to the thermal interactions between the built structures and their surroundings. To represent this relationship accurately in a microscale climate model, one must understand various aspects of heat transfer and the resulting thermodynamic and climatic effects.

a. Heat Absorption and Radiation

Walls, depending on their material and colour, have the capacity to absorb a substantial amount of shortwave solar radiation during the day. Dark-coloured surfaces or those with high absorptivity tend to take in more solar energy. Based on the insulation of the wall, some of this energy is transferred to the inner layers of the wall and then to the indoor environment, resulting in higher temperatures in the building or increased energy demand for cooling systems to maintain a given temperature level. Both aspects can be considered in ENVI-met.

These walls release stored energy back into the environment in the form of infrared radiation or convective heat transfer at the building facade when the ambient temperature drops, particularly at night. This occurrence contributes to the Urban Heat Island (UHI) effect, where urban areas experience notably higher temperatures than rural areas, specifically at night.

b. Heat Conduction

Heat transfer through walls occurs through conduction, either from the outer to the inner surface or vice versa. The efficiency of this process is influenced by the wall's thermal conductivity. Materials with high thermal conductivity, such as metals, conduct heat rapidly, which can affect the temperature of adjacent indoor and outdoor spaces. For an accurate representation of a building's thermodynamics in a numerical model, it is essential to define the thermal properties of the building's materials as accurately as possible. This can frequently be a challenge, particularly for older buildings with unknown wall structures.

Reflectivity and multiple reflections

Highly reflective walls, including those with mirrored or pale finishes, can bounce back a significant amount of shortwave radiation. This reflected energy can be absorbed by nearby structures, resulting in indirect heating. However, if only a few isolated buildings have such exteriors, unexpected environmental interactions can occur, amplifying the radiation's impact on nearby surfaces and objects. Using the *Indexed View Sphere* Algorithm (Simon et al., 2021), ENVI-met can accurately resolve multiple reflections for both shortwave and longwave radiation (refer to the following section).

d. Urban Canyons and Mutual Heating

In densely packed urban areas, the mutual radiation between walls of adjacent buildings can trap heat, especially in narrow alleys or streets. This scenario creates what is known as 'urban canyons,' where heat is continually exchanged between opposing surfaces, reducing the rate at which cooling can occur. This effect is relevant both for shortwave radiation as mentioned above, but especially during night, longwave thermal radiation that cannot escape into the free atmosphere due to horizon obstruction cause additional thermal heat load.

These are only a few aspects highlighting the importances and complexity of the impact of building walls and roofs on urban microclimate that need to be addressed in the model.

1.2 About this paper

This paper describes the new dynamic high-resolution wall and roof model as it is implemented in ENVI-met 5 and higher. **Parts 1** deals with the general design of the wall model and the numerical solution algorithms. Inspired by Terjung and O'Rourke's research in the early 1980s (Terjung and O'Rourke, 1980), ENVI-met employs a transient state model with multiple nodes to determine the surface temperatures of walls and roofs (referred to only as "walls" hereafter) and the allocation of heat inside such walls. It replaces previous algorithms, such as the steady-state approach utilized in versions up to and including V3.1, or the 3-Node model utilized in version v4.0, where a wall was viewed as a uniform structure made up of a single homogeneous material with physical characteristics such as heat capacity, thermal conductivity, absorption or emissivity.

In this paper, we present the ENVI-met wall model for bare walls. The model includes the basic equation for calculating wall surface temperatures and notes on its numerical solution.

Vegetated roofs and walls are vital elements in green building design and mitigating heat stress in urban settings. Therefore, it is crucial to offer a realistic simulation of these special wall systems in ENVI-met. The green wall model adds an additional model system in front of the building wall or roof. The model's detailed explanation can be found in part 2 of this technical documentation.

2 Calculation of the wall temperatures

2.1 Basic concept of the wall and roof model

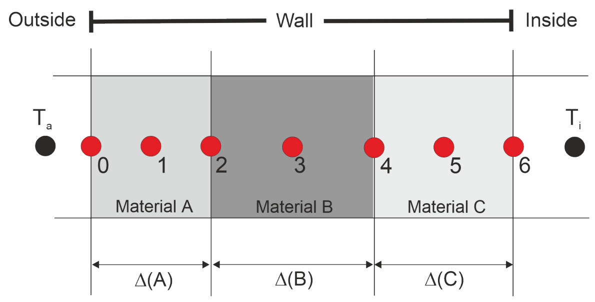

Figure 1: Basic concept of the new wall model with three different layers of material and seven prognostic calculation nodes T_0 to T_6

The wall and roof model (hereafter only *wall model*) as it is implemented in ENVI-met Version 5 and newer treats the wall as a sandwich out of three different layers of materials (see Figure 1). Each layer is represented by its physical material properties such as heat capacity, heat conductivity or transparency. The temperature of each layer of the wall is controlled by three calculation points: one in the center of the layer and one on each side of the layer interfacing to the next layer or to the outdoor or indoor air.

In total, the wall model is composed out of 7 calculation points T_0 to T_6, in which T_0 represents the outside facade surface and T_6 is the indoor surface of the wall. T_1 to T_5 are interior points in the wall. If it turns out to be necessary in later version, the model can easily be extended by further layers using the same concept described in this paper.

The handling of the ENVI-met database has been updated accordingly to support the features of the new wall model. The materials section allows to create new materials or edit material parameters including absorption, transmission, reflection, emissivity, specific heat capacity, thermal conductivity and density. The wall section allows to manually create or edit walls that now consist out of three different materials. The thickness and type of materials can be adjusted freely (see Figure 2).

2.2 The prognostic wall temperature equations

The temperature evolution at node i due to heat transfer inside wall material is given by the Fourier equation of molecular heat transfer. Although building walls are three-dimensional systems, and heat flows in any direction where temperature gradients are possible, the heat transfer inside the wall is treated only in one dimension in ENVI-met due to numerical limitations, focusing on the main gradient direction perpendicular to the wall surface.

Hence, we define the heat transfer equation as the Fourier-Equation in one dimension:

$$\frac{\partial T_i}{\partial t} = \kappa_i \frac{\partial^2 T}{\partial \Delta^2} \tag{2.1}$$

where κ_i is the relevant thermal diffusivity at node i in $[\mathrm{m}^2\mathrm{s}^{-1}]$ and Δ is the distance between the calculation nodes inside the wall.

Discretising the Fourier-Equation for a Finite-Difference scheme of the wall, the equation in implicit form solved forward in time becomes

$$\frac{T_i^* - T_i}{\Delta t} = \frac{1}{\Delta_{ic}} \left[\kappa_{i-} \left(\frac{T_{i-1}^* - T_i^*}{\Delta_{i-}} \right) - \kappa_{i+} \left(\frac{T_i^* - T_{i+1}^*}{\Delta_{i+}} \right) \right] \tag{2.2}$$

in which T_i^* denotes the temperature at node i for the future time step $t^* = t + \Delta t$ while T_i is the (known) temperature for the actual time t. This scheme now allows to distinguish the thermal diffusivity κ_{i-} between nodes $i-1$ and i and the diffusivity κ_{i+} between nodes i and $i+1$ which becomes relevant if the wall is composed out of different material layers.

Calculation of discrete node distances and thermal diffusivities

For the nodes in the middle of a material layer (nodes i=2,4 and 6, compare Fig. 1) the center, left and right differences (Δ_{ic},Δ_{i-} and Δ_{i+}) are equal to half the thickness of the assigned material layer.

For $i = 3$ in the center of material B as an example the differences are:

$$\Delta_{3-} = \Delta_{3c} = \Delta_{3+} = 0.5\Delta(B)$$

and analogous for $i = 1$ and $i = 5$.

The finite differences for the nodes located at the interfaces of the three material layers (nodes $i = 2$ and $i = 4$) are calculated with respect to the thickness Δ of adjacent layers. For node $i = 2$ the differences are:

$$\Delta_{2-} = 0.5(\Delta(A)) \tag{2.3}$$

$$\Delta_{2+} = 0.5(\Delta(B)) \tag{2.4}$$

$$\Delta_{2c} = 0.5(\Delta_{2-} + \Delta_{2+}) \tag{2.5}$$

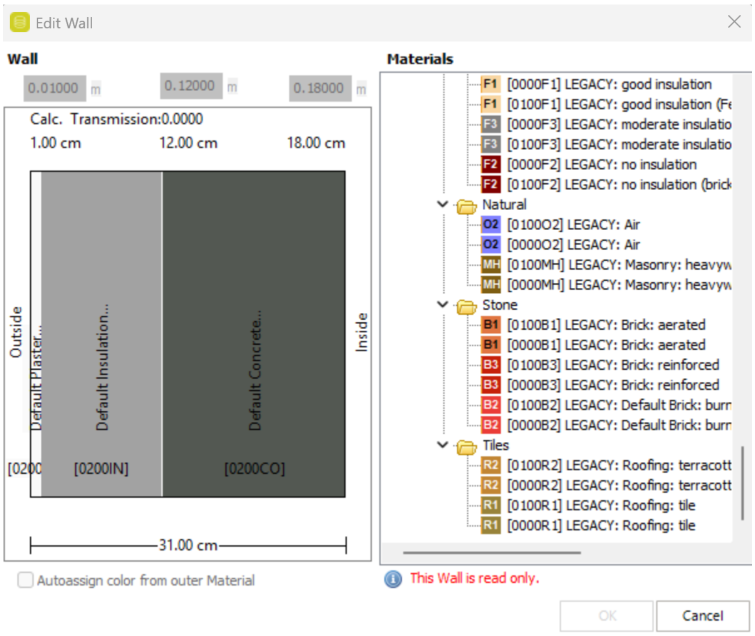

Figure 2: Dialog to create or alter the composition of walls / roofs

and analogous for $i = 4$.

The thermal diffusivity κ for the backward (-) and forward (+) exchange between the nodes i, $i-1$ and $i+1$ has to be calculated based on the materials layers involved in the process:

$$\begin{aligned}
\kappa_{0+}, \kappa_{1-}, \kappa_{1+}, \kappa_{2-} &= \lambda(A) \cdot \rho c_p(A)^{-1} \\
\kappa_{2+}, \kappa_{3-}, \kappa_{3+}, \kappa_{4-} &= \lambda(B) \cdot \rho c_p(B)^{-1} \\
\kappa_{4+}, \kappa_{5-}, \kappa_{5+}, \kappa_{6-} &= \lambda(C) \cdot \rho c_p(C)^{-1}
\end{aligned}$$

in which $\lambda(A/B/C)$ is the heat conductivity of wall material A, B or C and $\rho c_p(A/B/C)$ is the volumetric heat capacity calculated as the product of specific heat c_p and density ρ of the respective material.

Internal heat sources

The current wall model concept neglects possible heat gain within the material by absorption of short wave radiation, except for the external facade node. Consequently, shortwave radiation that penetrates the outer surface is not considered in the other two layers of the wall.

In theory, material compositions could exist where the maximum radiation absorption occurs in the middle or inner material layer. However, in such situations, the material layers are typically quite thin, allowing for the heat conduction to correct the error introduced by this assumption. For example, in the case of glass brick walls, the absorption caused by the middle and inner layers of material will be as small compared to the outer layer, so no significant error should be introduced here.

2.3 Boundary conditions of the walls system: Outer facade T_0

To solve the system of equations, boundary conditions are required for both the inner and the outer surface of the wall. Starting with the more complex outer surface (facade or roof), the energy budget of node 0 needs to be solved to satisfy an energy equilibrium $\cong 0$.

The energy budget equation for T_0 can be written as:

$$Q^{\mathrm{W}}_{\mathrm{SW,net}} + Q^{\mathrm{W}}_{\mathrm{LW,net}} - H^{\mathrm{W}} - LE^{\mathrm{W}} - G^{\mathrm{W}} \cong 0 \qquad (2.6)$$

where $Q_{\mathrm{SW,net}}$ are the shortwave radiative fluxes absorbed at the outer surface of the wall and $Q_{\mathrm{LW,net}}$ is longwave radiation budget of the outer facade.

H^{W} is the turbulent exchange of sensible heat with the air layer adjacent to the wall (see 2.3.2). LE^{W} is the (potential) energy change due to evaporation or condensation of vapour at the the wall material.

Finally, G^{W} is the heat conduction from/to the next calculation node T_2 inside the wall (see 2.3.3) .

Note: As a convention, the radiative fluxes are counted positive if energy is gained at the surface while the turbulent and conductive fluxes are counted positive when a loss of energy is taking place. These conventions are taken into account in the formulation of the surface energy budget equation.

Further Note: In the presence of wall or roof greening systems, the meaning of these variable will change as the vegetation and/or substrate layer will take the position of the air layer assumed here (see Part II of this documentation).

2.3.1 Radiative Components $Q^{\mathrm{W}}_{\mathrm{SW,net}}$ and $Q^{\mathrm{W}}_{\mathrm{lw,net}}$

The available **shortwave radiation** Q_{SW} at the wall segment is provided as a boundary condition using the main ENVI-met algorithms taking into account different aspects such as shading, sky visibility, reflection or transmission through semi-opaque objects such as trees. It can be further modified by attached greening systems.

The shortwave fluxes at the wall interface are distinguished into:

- Direct component $Q_{\mathrm{SW,dir}}$ from the sun
- Diffuse component $Q_{\mathrm{SW,dif}}$ from the sky
- Reflected component $Q_{\mathrm{SW,refl}}$ from the environment.

The shortwave radiation absorbed at the facade is calculated as

$$Q^{\mathrm{W}}_{\mathrm{SW,net}} = \tau_M \cdot (\cos(\beta) \cdot Q_{\mathrm{SW,dir}} + Q_{\mathrm{SW,dif}} + Q_{\mathrm{SW,refl}}) \tag{2.7}$$

where τ_M is the absorption coefficient of the outer wall material M and β is the three-dimensional angle between the normal of the facade surface and the incoming solar radiation.

If $\cos(\beta)$ becomes negative or β is larger than 90 degrees, the direct sun is hidden by the wall and the direct component is set to zero.

The longwave radiation budget is given as

$$Q^{\mathrm{W}}_{\mathrm{lw,net}} = Q_{\mathrm{lw}} - \Big((1-\varepsilon_M)Q_{\mathrm{lw}} + \varepsilon_M \cdot \sigma_B T_0^4\Big) \tag{2.8}$$

Like for the shortwave fluxes, the **longwave radiation** Q_{lw} at the wall element is provided by the ENVI-met main model taking into account the longwave counter radiation from the sky and the infrared radiation of objects *seen* by the wall segment.

Like for the shortwave fluxes, the accuracy of these data depend on the radiation scheme used in the model. The best results will be obtained using the *Indexed View Sphere* (IVS) algorithm (compare Simon et al., 2021).

In the presence of a Green Wall System (GWS), the incoming longwave fluxes will not be taken directly from the ENVI-met model, but will be modified by the GWS like for all other variables.

2.3.2 Sensible Heat Flux H^{W}

The turbulent flux of sensible heat H^{W} is driven by the temperature difference between the facade surface T_0 and the ambient air temperature in front of the facade T_a.

$$H^{\mathrm{W}} = c_p\rho \cdot K_h^w \frac{T_0 - T_a}{\Delta_{\mathrm{W}}} \tag{2.9}$$

Here, K_h^w is the exchange coefficient for heat at the wall surface and Δ_{W} is the distance between the wall and the position of the calculation point for the air temperature, usually the half grid size in the direction of the facade surface normal.

Alternativly, the turbulent flux can be expressed using a convection coefficient h_c which leads to the equivalent formulation

$$H^{\mathrm{W}} = h_c\,(T_1 - T_a) \tag{2.10}$$

Since ENVI-met Version 4.4, two different formulations can be used to calculate the heat transfer at the Wall: The formulation from German DIN 6946 (default setting) and the classical formulation based on the similarity theory of Monin-Obukov (1954), that is also used to calculate the heat and vapour fluxes at the soil surface.

Sensible heat flux with DIN 6946

According to German DIN 6946, the sensible heat flux is only a function of the temperature difference and the wind speed along the facade:

$$h_c = 4 + 4\mathbf{u} \tag{2.11}$$

where $\mathbf{u}$ is the tangential wind velocity above the wall surface of interest.

Sensible heat flux with Monin-Obukov

Applying the similarity theory of Monin-Obukov to the surface takes into account additional parameters of the surface such as the roughness length of the surface and, in the case of horizontal surfaces, the thermal stratification between the facade surface and air.

To apply the similarity theory, we write the turbulent sensible heat flux as:

$$H^{\mathrm{W}} = c_p\rho_a \cdot K_h^w \frac{T_0 - T_a}{\Delta_w} = c_p\rho \cdot u_*\theta_* \tag{2.12}$$

in which u_* is the friction velocity at the wall surface and θ_* is the scaling temperature for the heat flux.

Using the drag coefficient c_D the Monin-Obukov flux $u_*\theta_*$ can be written as

$$u_*\theta_* = c_D \cdot \mathbf{u} \cdot (T_0 - T_a) \tag{2.13}$$

which is valid for neutral conditions and/or vertical walls.

The drag coefficient is defined as

$$c_D = \frac{\kappa^2}{\left(\ln\left(\Delta_\mathrm{W} + z_0^w\right)/z_0^w\right)^2} \tag{2.14}$$

where κ is the von-Karman constant (=0.4) and z_0^w is the roughness length of the wall surface.

For horizontal walls, the thermal stratification can be taken into account by adding a stability function Φ_h:

$$u_*\theta_* = c_d \cdot \mathbf{u} \cdot \Phi_h\left(Ri_b\right) \cdot (T_0 - T_a) \tag{2.15}$$

The stability function itself is defined as:

$$\Phi_h(Ri_b) = \begin{cases} 1 - \frac{bRi_b}{1+c_h|Ri_b|^{0.5}} & ; Ri_b < 0 \\ n_h & ; Ri_b = 0 \\ \left(1 + aRi_b\right)^{-2} & ; Ri_b > 0 \end{cases} \tag{2.16}$$

with the coefficients

$$a = 4.7 \qquad b = 9.4$$
$$n_h = 1.35$$
$$c_m = 7.4 \cdot c_d \cdot b\left(\Delta_\mathrm{W}/z_0^w\right)^{0.5} \qquad c_h = 0.72 \cdot c_m$$

These coefficients are based on universal stability functions and are generally accepted for microscale exchange processes (see e.g. Stull, 1994; Asaeda and Thanh Ca, 1993).

Finally, the bulk Richardson-Number Ri_b is given as

$$Ri_b = \frac{g \cdot \Delta_\mathrm{W}\left(T_a - T_0\right)}{0.5\left(\theta_a + T_1\right)\mathbf{u}^2} \tag{2.17}$$

When required, the exchange coefficient K_h^w can be calculated as:

$$K_h^w = \Delta_\mathrm{W} \cdot c_D \cdot \mathbf{u} \cdot \Phi_h \tag{2.18}$$

The relation between K_h^0 and h_c is given by

$$\frac{h_c \cdot \Delta_\mathrm{W}}{c_p\rho_a} = K_h^w \Leftrightarrow h_c = K_h^w \frac{c_p\rho_a}{\Delta_\mathrm{W}} \tag{2.19}$$

2.3.3 Conductive Heat Flux G^W

The heat conduction G_w between the outer surface and the neighbouring inner node T_1 can be easily calculated using the material properties of material A and the temperature node T_1. G_w is then given by

$$G^\mathrm{W} = \frac{\lambda(A)}{0.5\Delta(A)}\left(T_0 - T_1\right) \tag{2.20}$$

2.4 Boundary conditions of the walls system: Inner wall surface T_6

In principle, the same concept described for calculating the outside facade temperature T_0 applies for the inner wall surface temperature T_6.

For the indoor wall, a number of assumption must be made to reduce the complexity of the methode. The most important assumption here is that radiative transfers between inner walls are neglected in the energy balance. As the model does not include detailed information on indoor surfaces such as the floor, inner walls or furniture, we assume that all other surfaces seen by node 6 have more or less the same temperature. Moreover, the reflection of shortwave radiation inside the building is not taken into account.

As a consequence of this simplification, we can ignore the net absorbed shortwave radiation at T_6 and we can also assume that longwave radiation budget equals zero due to an isothermal indoor environment. With this assumptions, we can write the energy budget equation for node T_6 as

$$G^\mathrm{W} - H^\mathrm{W} \cong 0 \tag{2.21}$$

where G^W is the conduction heat flux between T_5 and the inner wall surface node T_6 with

$$G^\mathrm{W} = \frac{\lambda(C)}{0.5\Delta(C)}\left(T_5 - T_6\right) \tag{2.22}$$

counted positive in the case of heat transfer towards T_6.

H^W is the sensible heat transfer between the inner wall surface and the indoor air with

$$H^\mathrm{W} = h_i\left(T_6 - T_\mathrm{indoor}\right) \tag{2.23}$$

The heat transfer coefficient h_i for the inner wall is taken constant in the simulation. Following DIN 6946, H_i is composed out of a convective and a radiative exchange component:

$$h_i = h_{c,i} + h_{r,i}$$

For vertical walls, the convective component $h_{c,i}$ is set to 2.5 $\left[\mathrm{W\,m^{-2}\,K^{-1}}\right]$ and the radiative component $h_{c,r}$ is assumed to be $0.9 \cdot 5.7 = 5.2$ $\left[\mathrm{W\,m^{-2}\,K^{-1}}\right]$ for an indoor temperature around 20 °C and a wall emissivity of 0.9, resulting in an overall h_i of 7.7 $\left[\mathrm{W\,m^{-2}\,K^{-1}}\right]$.

For horizontal walls, we set $h_{c,i} = 5.0$ $\left[\mathrm{W\,m^{-2}\,K^{-1}}\right]$ and $h_{r,i} = 5.2$ $\left[\mathrm{W\,m^{-2}\,K^{-1}}\right]$ which sums to $h_i = 10.2$ $\left[\mathrm{W\,m^{-2}\,K^{-1}}\right]$

2.5 Interface to the atmosphere model

2.5.1 Radiative Fluxes

The **outgoing radiative fluxes** (shortwave $Q^{\text{ret}}_{\text{SW,dif}}$ and longwave $Q^{\text{W}}_{\text{LW,out}}$) from the wall back to the atmosphere are calculated as:

$$Q^{\text{ret}}_{\text{SW,dif}} = \alpha_{\text{W}} \cdot \Big(Q_{\text{SW,dir}} \cdot \cos(\beta) + Q_{\text{SW,dif}} + Q_{\text{SW,refl}}\Big) \tag{2.24}$$

Note, that the outgoing shortwave radiation is handled as diffuse radiation, hence no directed reflection is supported by the model.

The outgoing longwave flux can be written as:

$$Q^{\text{W}}_{\text{LW,out}} = (1 - \varepsilon_{\text{W}}) \cdot Q_{\text{LW}} + \sigma_B \cdot \varepsilon_{\text{W}} \cdot T^4_{\text{W},0} \tag{2.25}$$

2.5.2 Turbulent Heat Flux

In the main atmosphere model of ENVI-met, the **heat flux** from or to a wall S_θ is introduced as an additional source/ sink term in the prognostic equations of the temperature field:

$$S_\theta = K^w_h \frac{T_0 - T_a}{\Delta^2_{\text{W}}} \tag{2.26}$$

where S_θ is defined positive for a heat flux from the wall to the atmosphere.[1]

In addition, T_0 will be provided as the relevant wall temperature in order to calculate the longwave fluxes emitted to the environment and the reflected shortwave radiation is returned to the IVS radiation model.

Please note, that in the case of vegetated walls, both T_0 and K^w_h will be replaced by different values calculated for the Green Wall System (see Part 2 of this paper).

3 Solving the wall temperature system

The first step for obtaining updated temperature distribution in a given wall consists of the iterative solution of the energy budget for the outer (eq. 2.6) and inner facade surface nodes (eq. 2.21) using the different fluxes discussed in the previous sections.

The energy balance equations are solved iteratively to find an energy budget $\cong 0$ using the Regula-Falsi method that provides a superlinear convergence especially if the initial guesses are not too wrong. This is normally the case for a relatively inert system like a building wall. Moreover, Regula-Falsi does not require the analytical formulation of the first derivate of the energy balance equation which keeps the approach open for much more complicated systems in which the derivates cannot be calculated.

The balanced energy equations provide updated temperatures T^*_0 and T^*_6 for the both surfaces that can then be used as boundary conditions to solve the system of Fourier Equations leading to the new inner wall temperatures T^*_1 to T^*_5. Please note, that lateral heat transfer between neighboring wall segments is not taken into account in the model due to its one-dimensional nature.

For each wall segment in the model, the above procedure needs to be executed using relatively small update intervals. Hence, the numerical methods applied have a high impact on the overall numerical performance of the simulation model.

3.1 Solving the Fourier-Equations for the inner nodes

The Fourier-Equations as shown in the later sections provide a system of linked equations defining the temperature dynamics at the inner wall nodes T_1 to T_5. In general, this system can be solved in either an explicit or an implicit way. While the explicit solution is easy to calculate, it tends to be numerically unstable and requires small time steps, especially if the material is thin and/or the heat conduction is fast (glass or metal walls). The implicit solution of the equation system is numerically more expensive, but allows larger time step and has only little tendency to generate unstable solutions. As most of the prognostic equations in ENVI-met are solved implicitly, an implicit solution of the wall temperature system was chosen.

Mathematical Toolbox

Solving the Fourier-Equation or any other partial differential equation (PDE) with an implicit numerical method requires more work in terms of preparing the equation to make it solvable and some more understanding of the

1. If the atmospheric pressure in the model is not equal to standard pressure of 1013 hPa, potential air temperature θ and absolute temperature T must be converted accordingly when used together.

principles of solving linked equation systems. We have the impression, that there are only very few papers that explain and illustrate the process of equation solving, most of them just give the PDE to explain the physics behind the problem and then present the results. For this reason, we have decided to use this paper to illustrate the mathematical background when using a PDE system as a proxy for almost all numerical methods used in ENVI-met.

This also to give credit to the paper of Terjung and O'Rouke (Terjung and O'Rourke, 1980) who simulated the casual elements of the urban heat island long before numerical models established as a state-of-the art tool. In their paper, they also presented widely the numerical procedures they used and we will forward this in our documentation here.

3.1.1 Assembling the equations

Setting up the equations for the implicit solution process starts with the finite difference discretisation of the Fourier-Equation written for an internal wall node i:

$$\frac{T_i^* - T_i}{\Delta t} = \frac{1}{\Delta_{ic}}\left[\kappa_{i-}\left(\frac{T_{i-1}^* - T_i^*}{\Delta_{i-}}\right) - \kappa_{i+}\left(\frac{T_i^* - T_{i+1}^*}{\Delta_{i+}}\right)\right] \tag{3.1}$$

Rearranging the equation we get

$$\frac{T_i^* - T_i}{\Delta t} = \frac{\kappa_{i-}}{\Delta_{ic}\Delta_{i-}}\left(T_{i-1}^* - T_i^*\right) - \frac{\kappa_{+}}{\Delta_{ic}\Delta_{i+}}\left(T_i^* - T_{i+1}^*\right) \tag{3.2}$$

For application in a matrix solver and for better readability we substitute A and C in which A represents the exchange processes taking place between node i and its left (downward) neighbour $i-1$ and C is the counterpart for processes with the right (upward) neighbour $i+1$:

$$A_i = \frac{\kappa_{i-}}{\Delta_{ic}\Delta_{i-}} \text{ and } C_i = \frac{\kappa_{i+}}{\Delta_{ic}\Delta_{i+}}$$

Now, we substitute A and C into the restructured equation (3.2) and we get

$$\left(T_i^* - T_i\right)\Delta t^{-1} = A_i\left(T_{i-1}^* - T_i^*\right) - C_i\left(T_i^* - T_{i+1}^*\right) \tag{3.3}$$

Next, we break up the brackets and sort for the future node temperatures T_i^*, T_{i-1}^* and T_{i+1}^*

$$T_i^* \cdot \Delta t^{-1} - T_i \cdot \Delta t^{-1} = A_i \cdot T_{i-1}^* - (A_i + C_i) \cdot T_i^* + C_i \cdot T_{i+1}^* \tag{3.4}$$

On the left hand side, $T_i^* \Delta t^{-1}$ must be moved to the right hand side of the equation:

$$-T_i \cdot \Delta t^{-1} = A_i \cdot T_{i-1}^* - (A_i + C_i + \Delta t^{-1}) \cdot T_i^* + C_i \cdot T_{i+1}^*$$

Finally, we simplify the equation with another substitution that is $B_i = A_i + C_i + \Delta t^{-1}$ and inverse the signs of the equation so we get

$$T_i \cdot \Delta t^{-1} = -A_i \cdot T_{i-1}^* + B_i \cdot T_i^* - C_i \cdot T_{i+1}^* \tag{3.5}$$

In this form, the equation system for a one-dimensional system of nodes $i = 0..6$ can be interpreted straight forward as a vector-matrix system in the form

$$\mathbf{y} = M \cdot \mathbf{x}$$

in which the vector $\mathbf{y}$ represents the known values at the nodes i at a given time step t (in this case the old temperature values at nodes 0 to 6), the $\mathbf{x}$ vector contains the unknown and required values at the corresponding nodes (the new temperature values at nodes 0 to 6). Finally, M is the coefficient matrix linking the different nodes of the system with each other and containing A, B and C in our case.

3.1.2 Solving the equation system

Obviously, the implicit solution of the equation system given above requires the simultaneous solution of all nodes involved in the observed system and therefore generates an equation system of N linearly independent equations which needs to be solved.

Formally, the solution of the vector-matrix equation system as given above

$$\mathbf{y} = M \cdot \mathbf{x}$$

can be achieved by rearranging the equation as

$$\mathbf{x} = M^{-1} \cdot \mathbf{y}$$

Here, M^{-1} is the inverse of the coefficient matrix which will be composed in detail in the following section. The calculation of this inverse matrix is the core task of the numerical solver for this equation system. Once M^{-1} is known, the required values $\mathbf{x}$ can easily be obtained through matrix-vector multiplication.

In the first step, we define vector $\mathbf{y}$ holding the known right hand side value of the inner wall nodes based on equation 3.5:

$$\mathbf{y} = \begin{bmatrix} \sqcup \\ T_2 \cdot \Delta t^{-1} \\ T_3 \cdot \Delta t^{-1} \\ T_4 \cdot \Delta t^{-1} \\ T_5 \cdot \Delta t^{-1} \\ T_6 \cdot \Delta t^{-1} \\ \sqcup \end{bmatrix} \begin{matrix} i = 0 \text{ (outside)} \\ i = 1 \\ i = 2 \\ i = 3 \\ i = 4 \\ i = 5 \\ i = 6 \text{ (inside)} \end{matrix}$$

For the boundary nodes $i = 0$ and $i = 6$, the entries are marked with $\sqcup$ and will be added later.

The solution vector $\mathbf{x}$ will contain the required future values at all nodes after time step $t + \Delta t$:

$$x = \begin{bmatrix} T_0^* \\ T_1^* \\ T_2^* \\ T_3^* \\ T_4^* \\ T_5^* \\ T_6^* \end{bmatrix} \begin{matrix} i = 0 \\ i = 1 \\ i = 2 \\ i = 3 \\ i = 4 \\ i = 5 \\ i = 6 \end{matrix}$$

Finally, the coefficient matrix M needs to be set up based on the structure of eq. 3.5 and the definition of A_i, B_i, and C_I in which the empty elements equal zero. :

$$M = \begin{bmatrix} \sqcup & \sqcup & & & & & \\ -A_1 & B_1 & -C_1 & & & & \\ & -A_2 & B_2 & -C_2 & & & \\ & & -A_3 & B_3 & -C_3 & & \\ & & & -A_4 & B_4 & -C_4 & \\ & & & & -A_5 & B_5 & -C_5 \\ & & & & & \sqcup & \sqcup \end{bmatrix} \tag{3.6}$$

Boundary conditions of the system

Obviously, the Fourier-Equation and the resulting vector-matrix set of equations cannot be applied to the first and the last node in the system as it lacks neighbours.

Solving the boundary conditions for the given system is easy as the required temperatures of the outer (T_0^*) and inner (T_6^*) wall are calculated with their own methods outside the Fourier system and can be considered as known and given by the time the inner nodes are calculated.

Hence, we just insert the pre-calculated T_0^* and T_6^* into the $\mathbf{y}$ vector and set $B_0, B_6 = 1$ and $C_0, A_6 = 0$.

As final vector-matrix system we get:

$$\mathbf{y} = \begin{bmatrix} T_0^* \\ T_1 \cdot \Delta t^{-1} \\ T_2 \cdot \Delta t^{-1} \\ T_3 \cdot \Delta t^{-1} \\ T_4 \cdot \Delta t^{-1} \\ T_5 \cdot \Delta t^{-1} \\ T_6^* \end{bmatrix} \begin{matrix} i = 0 \\ i = 1 \\ i = 2 \\ i = 3 \\ i = 4 \\ i = 5 \\ i = 6 \end{matrix}$$

$$M = \begin{bmatrix} 1 & & & & & & \\ -A_1 & B_1 & -C_1 & & & & \\ & -A_2 & B_2 & -C_2 & & & \\ & & -A_3 & B_3 & -C_3 & & \\ & & & -A_4 & B_4 & -C_4 & \\ & & & & -A_5 & B_5 & -C_5 \\ & & & & & & 1 \end{bmatrix}$$

Inverting the coefficient matrix

To solve the equation system for x as the future temperature for all wall nodes, the calculation of the inverse matrix M^{-1} from M is required which is the most computational resource demanding step when solving the the prognostic wall temperature equation.

As only neighbouring points are numerically connected, the M matrix is a spare tridiagonal matrix which can me solved w.g in a single step using LU decomposition and forward- and backsubstitution (*Tridiagonal Matrix Algorithm* or *Thomas' Algorithm,* Thomas, 1949).

Once the inverse matrix is calculated, the new temperature values can be directly obtained by multiplication with the y vector as written above with

$$\mathbf{x} = M^{-1} \cdot \mathbf{y}$$

Numerical efficiency

Obviously, the solution of the facade and wall temperature system is a model component that is constantly called during the model run. Hence, numerical optimization methods in this module will bring large benefits to the overall model performance.

In ENVI-met, each wall segment is programmed as an individual object carrying both its properties and calculation methods. All relevant physical properties are stored inside this object and wherever possible, constant derivatives are pre-calculated.

In the case of the matrix inversion process, we can see that both A and C are only defined using constant properties of the wall system. So, these coefficients can be pre-calculated and only B, which includes Δt which might change and the vector y must be updated each time the prognostic system for the wall temperatures is executed.

Figure 3: Aerial photo of the Fraunhofer Institute for Building Physics testing site and the facade temperature measurement -The red boxes indicate the measurement building (underlying picture, Source: Google Earth) / the location of the contact thermometer (top picture)

4 Evaluation of the multiple-node model by comparison with measurement data

4.1 Study site

To further validate the new implementations, evaluation simulations were conducted and compared against measurement data. In collaboration with the Fraunhofer Institute for Building Physics in Holzkirchen (IBP), the evolution of the surface temperature of a facade was compared against ENVI-met's model results. The IBP operates a building testing site where different building materials are measured in controlled environments (see Figure 3). The testing site is located in Holzkirchen, Germany (47.87°N, 11.73°E, elevation 680 m a.s.l.).

The facade for the comparison of the measured surface temperatures against the modeled surface temperatures can be seen in figure 3. The flat roof test building is 4 meters high, and 6 by 42 meters in width and length. In the lower part of the building, up until a height of 2 meters, the wall is uninsulated, while in the upper part the wall is insulated.

4.2 Monitored parameters & material properties

The surface temperature is continuously measured with a PT100 contact resistance thermometer on a south facing uninsulated part of the wall at a height of 0.6 meters (see Figure 3). In the temperature range between 0°C and +100°C the measurement accuracy of the PT100 contact thermometer should lie at ±0.3 Kelvin.

All structural information such as the material composition of the walls as well as the physical parameters of components were provided by the IBP (Table 1).

Table 1: Material properties of the components of the measured facade

	Wall component		
	exterior plaster	brickwork	interior plaster
Material	exterior plaster	brick	lime plaster
Thickness [m]	0.02	0.505	0.015
Thermal conductivity [W m^{-1} K^{-1}]	0.87	0.21	0.70
Density [kg m^{3}]	1310	700	1600
Specific heat capacity [J kg^{-1} K^{-1}]	850	1000	850

Additionally, meteorological data were measured on the testing site and provided by the IBP. The measured parameters - air temperature and humidity, wind speed, wind direction, shortwave radiation (direct and diffuse) and longwave radiation - were used as boundary conditions for ENVI-met.

4.3 ENVI-met boundary conditions & model area

Based on the meteorological measurement data and ENVI-met's full-forcing method, four simulation periods of several consecutive days were selected to provide boundary conditions for the microclimate model ENVI-met. To test the model under significantly different meteorological conditions and with and without a regulation of indoor air temperatures, the first two simulation periods were chosen to be in spring while the second two simulation periods covered several consecutive days in summer. During the spring periods the building was heated to an indoor air temperature of 20°C, while in the summer periods the building's indoor air temperature was not regulated. The combination of different meteorologies and the differences in the regulation of the indoor air temperature lead to a sophisticated test for the new multiple-node model.

To account for the heating during the spring periods, the indoor air temperature was set constant to 20°C for the spring simulations. In the summer simulations the indoor air temperature was prognosticly modeled using the approach shown above.

Table 2 shows the average meteorological conditions of the four simulation periods; Figure 4 shows the diurnal variations of the direct and diffuse shortwave radiation for the four simulation periods.

Table 2: Average meteorological conditions in 10 meters above ground for the four simulation periods

	Parameter		
	air temp.	spec. humidity	wind speed
Spring01 (19.-25.04.2015)	9.3°C	4.4 g kg^{-1}	2.6 m/s
Spring02 (09.-15.05.2015)	14.5°C	7.5 g kg^{-1}	2.7 m/s
Summer01 (03.-09.07.2014)	17.1°C	9.0 g kg^{-1}	3.4 m/s
Summer02 (14.-20.07.2014)	19.9°C	9.7 g kg^{-1}	1.9 m/s

Utilizing the material properties of the components of the measured facade and ENVI-met's advanced multiple-node model, the material properties and wall structure were reconstructed (Figure 5, left). Since the multiple-node model now features seven nodes, all three of the wall's components could be digitized without parametrization (see Figure 5, left). The albedo of the exterior plaster was set to 0.6, the emissivity to 0.9.

The model area covered 80 meters × 60 meters × 40 meters, its horizontal and vertical resolution was set to 2 meters (Figure 5, right).

4.4 Results and discussion

The comparison of the measured and the modeled facade temperatures shows a very high overall model fit for all simulation periods: $R^2 = 0.98$ for the Spring01 period, $R^2 = 0.96$ for the Spring02 period and $R^2 = 0.98$ and $R^2 = 0.99$ for the Summer01 and the Summer02 periods, respectively (see Table 3). The high R^2 values indicate that a very high percentage (96% to 99%) of the variation of the measured surface temperature can be explained by the model, i.e. that the shapes of the curves are remarkably similar.

Table 3: Model fit between measured and modeled facade temperatures

	model fit		
	R^2	RMSE [K]	NRMSE
Spring01 (19.-25.04.2015)	0.98	2.13	0.07
Spring02 (09.-15.05.2015)	0.96	1.71	0.06
Summer01 (03.-09.07.2014)	0.98	1.03	0.03
Summer02 (14.-20.07.2014)	0.99	1.25	0.05

Since high R^2 values do not automatically mean that the absolute values are closely matched between the model and the measurement, a second indicator, the root mean square error (RMSE) was calculated (see Table 3).

The RMSE accounts for the absolute differences between the simulated and the observed facade temperatures. However, it is dependent on the absolute values and can thus not be readily compared across the meteorological conditions. Therefore, a normalized RMSE (NRMSE) is calculated by dividing the RMSE by the range of measured values. This allows a direct comparison between the different meteorological conditions. The comparison of the RMSE of the measured and modeled facade temperatures for all simulation periods (Table 3) shows a large agreement in all meteorological conditions.

The generally very low RMSE - mostly below 2 Kelvin - in all four simulation periods, which feature significantly different outdoor and indoor conditions, corroborates the high accuracy of ENVI-met's multiple-node model. Comparing the NRMSE across the meteorological conditions reveals that simulation results are even more accurate in the two summer periods than in the two spring periods. This is probably due to the spring periods being more complex because of the indoor temperature regulation to 20°C.

Figure 6 shows a comparison of the diurnal variations of the measured and modeled surface temperatures as well as the delta between the two for all four simulation periods. For all simulation periods the measured and the modeled temperature curves demonstrate remarkable agreement between the modeled and the measured data. ENVI-met matches the daily variations of the surface temperatures very well, even slight variations are represented by the model.

The comparison of the diurnal variations corroborates the findings based on the NRMSE reported above and shows that the agreement between the modeled and measured facade temperatures in the summer periods is significantly better than in the spring periods. The general tendency to slightly underestimate the facade temperatures compared to the measurement values is larger in both spring periods where the absolute facade temperatures are lower and the indoor temperature is regulated to 20°C.

The highest discrepancies are found at around 14:00 where both the simulation and the measurement show the highest facade temperatures. Only on the second to last and the last day of the Summer01 period the model slightly overestimates the facade temperatures. This is most likely caused by small amounts of precipitation on these days. Since precipitation is not included in the model a latent heat flux reducing the surface temperature of the facade cannot be replicated in the model.

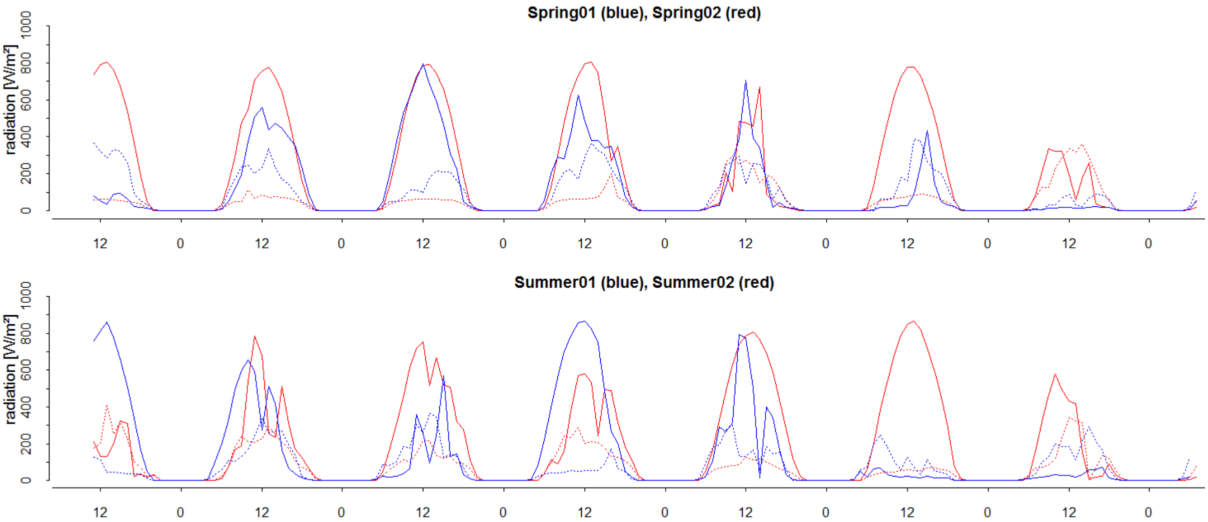

Figure 4: Diurnal variations of the direct and diffuse shortwave radiation of the four simulation periods

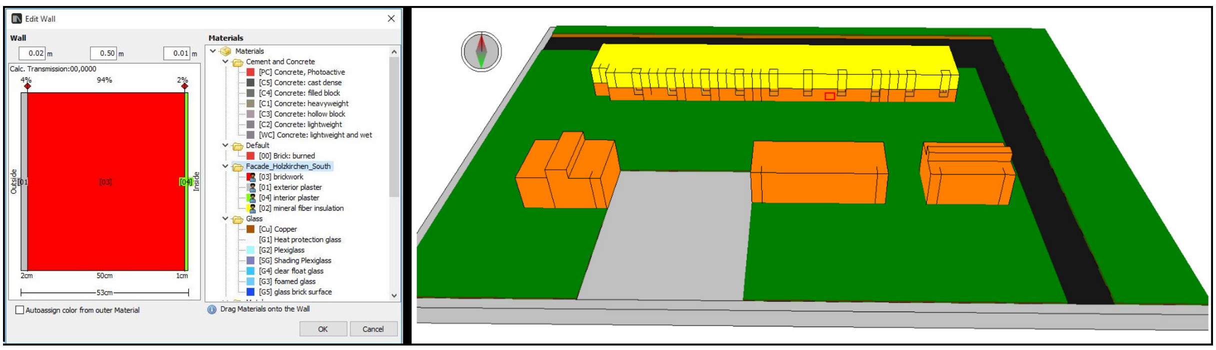

Figure 5: Left: Structure of the digitized uninsulated wall; Right: 3D visualization of the model area. The red box indicates the location of the contact thermometer

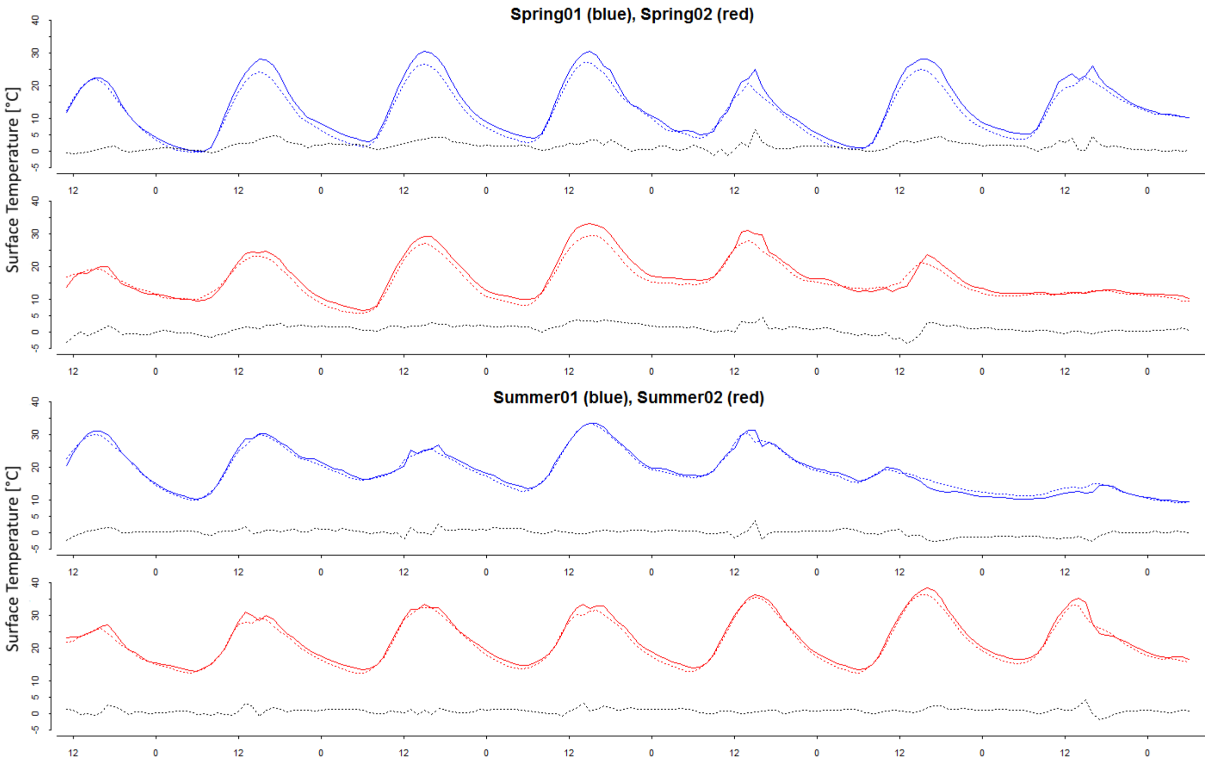

Figure 6: Comparison of the measured and modeled facade temperatures - Solid lines: measured data, dotted lines: modeled data, gray dotted line: difference between measured and modeled data values

5 Conclusion and outlook

The paper presents ENVI-met's advanced multiple-node wall and roof model, discussing its basic concept and its application to non-vegetated walls and roofs. The following section, Part 2, will introduce the concept of vegetated walls and roofs.

The newly implemented model enables digitization of more complex walls or roofs, featuring up to three different materials. In addition to the comprehensive 3D mode, where distinct wall and roof materials can be assigned to each building cell, ENVI-met enables in-depth analysis of building physics in intricate urban settings. Dividing buildings into separate zones, treated as confined air volumes, enables a rough estimation of indoor temperature. A proof-of-concept simulation demonstrated the capabilities of new implementations in simulating wall and roof temperatures, as well as Indoor Temperature estimation. The proof-of-concept simulations demonstrated ENVI-met's ability to produce reliable outcomes for the effects of varied wall materials on indoor air temperature. Additionally, the model effectively captures the influence of outdoor elements such as trees or other objects on facade temperatures.

The new implementations were assessed in relation to the measurement data provided by the Fraunhofer Institute for Building Physics Holzkirchen in a comparison of measured and modeled facade temperatures. To assess the model under various meteorological conditions, four distinct periods of consecutive days were simulated and compared against the measurement data. The initial two periods took place in the summer when the indoor air temperature of the building was unregulated. The following two periods happened in the spring, during which the indoor air-temperature was at 20°C. The assessment of the simulated temperatures of the building's facade aligned well with the measured facade temperatures, displaying exceptional accuracy. The simulation periods, which comprised the total of 24 days, were thus all satisfactory. The excellent findings support the superior precision of ENVI-met's wall and roof module. In general, the outcomes reveal that, thanks to the progress of the multi-node model, ENVI-met can replicate the physics of constructing procedures in complicated surroundings.

References

Asaeda, T. and Thanh Ca, V. (1993). The subsurface transport of heat and moisture and its effect on the environment:a numerical model. *Boundary Layer Meteorology*, 65:159–179.

Simon, H., Sinsel, T., and Bruse, M. (2021). Advances in Simulating Radiative Transfer in Complex Environments. *Applied Sciences*, 11(12):5449.

Stull, R. B. (1994). A convective transport theory for surface fluxes. *Journal for the Atmospheric Science*, 51(1):3–22.

Terjung, W. H. and O'Rourke, P. A. (1980). Simulating the causal elements of the urban heat islands. *Boundary Layer Meteorology*, 19:93–118.

Thomas, L. (1949). Elliptic problems in linear differential equations over a network. Technical report, Watson Sci. Comput. Lab Report, Columbia University, New York.